[Article] www.whxb.pku.edu.cn

新型锂盐 $LiBC_2O_4F_2$ 在 EC+DMC 溶剂中的电化学行为

高宏权 赖延清 张治安* 刘业翔

(中南大学冶金科学与工程学院, 长沙 410083)

摘要: 采用差热-热重(TG-DTA)、恒电流充放电和交流阻抗(EIS)分析了二氟草酸硼酸锂(LiODFB)的热稳定性, 研究了 LiODFB/碳酸乙烯酯(EC)+碳酸二甲酯(DMC)电解液的电化学性能及界面特征. 实验结果表明, LiODFB 不仅具有更高的热稳定性, 而且在 EC+DMC 溶剂中具有较好的电化学性能. 与使用 $LiPF_6$/EC+DMC 的电解液相比, 锂离子电池应用 LiODFB 基电解液在 55 ℃的高温具有更好的容量保持能力; 以 0.5*C*、1*C*(1*C*=250 mA·g^{-1})倍率循环放电, 两种电池间的倍率性能差别较小; LiODFB 能够在 1.5 V(*vs* Li/Li$^+$)左右在石墨电极表面还原形成一个优异稳定的保护性固体电解质相界面膜(SEI 膜); 交流阻抗表明, 使用 LiODFB 基电解液的锂离子电池仅具有稍微增加的界面阻抗. 因此 LiODFB 是一种非常有希望替代 $LiPF_6$ 用作锂离子电池的新盐.

关键词: 锂离子电池; 电解液; 二氟草酸硼酸锂; 电化学性能; 界面特性

中图分类号: O646

Electrochemical Behaviors of New Lithium Salt $LiBC_2O_4F_2$ in EC+DMC Solvents

GAO Hong-Quan LAI Yan-Qing ZHANG Zhi-An* LIU Ye-Xiang

(*School of Metallurgical Science and Engineering, Central South University, Changsha 410083, P. R. China*)

Abstract: The thermal stability of lithium difluoro(axalato)borate (LiODFB) was analyzed by thermal gravimetric-differential thermal analysis (TG-DTA). The electrochemical performance and interfacial characteristics of the LiODFB/ethylene carbonate (EC)+dimethyl carbonate (DMC) electrolyte were studied by constant current charge-discharge and electrochemical impedance spectroscopy (EIS). Results show that LiODFB has higher thermal stability and that the lithium-ion cells using LiODFB salt in EC+DMC solvents exhibit excellent electrochemical performances. Compared with the $LiPF_6$/EC+DMC electrolyte, the lithium-ion cells using LiODFB-based electrolyte have very good capacity retention at 55 ℃. At 0.5*C* and 1*C* (1*C*=250 mA·g^{-1}) discharge rates, the difference between the rate capability of the two cells is tiny. LiODFB is reduced at about 1.5 V (*vs* Li/Li$^+$) and forms a robust protective solid electrolyte interphase (SEI) film on the graphite surface. EIS tests show that these lithium-ion batteries which use the LiODFB-based electrolyte have a slightly higher interfacial impedance. Therefore, as a new salt, LiODFB is a promising alternative lithium salt for the replacement of $LiPF_6$ in lithium ion battery electrolytes.

Key Words: Lithium-ion battery; Electrolyte; Lithium difluoro(axalato)borate; Electrochemical performance; Interfacial property

Recent advances in cathode and anode materials have refocused attention on electrolytes as the technological bottleneck limiting the operation and performance of lithium-ion battery systems. Whereas, attributes such as cell potential and energy density are related to the intrinsic property of the positive and negative electrode materials, cell power density, calendar-life

Received: November 20, 2008; Revised: January 19, 2009; Published on Web: March 3, 2009.

*Corresponding author. Email: zhianzhang@sina.com; Tel: +86731-8876454.

国家科技支撑计划(2007BAE12B01)及国家自然科学基金项目(20803095)资助

and safety are dictated by the nature and stability of the electrolyte and the electrode-electrolyte interface[1,2]. Lithium-ion battery electrolytes of commercialization typically consist of lithium hexafluorophosphate ($LiPF_6$) dissolving in mixture solvents of ethylene carbonate (EC)+dimethyl carbonate (DMC). The high dielectric constant cyclic EC enables the dissolution of lithium salts to sufficient concentrations, and possesses good compatibility with graphite electrode, but is rather viscous. The linear DMC, on the other hand, is low dielectric constant but its low viscosity and broader temperature window promote rapid ion transport. So they are chosen as components of most lithium-ion battery electrolytes of commercialization. The commonly used $LiPF_6$ is the salt of the main choice for lithium-ion batteries of commercialization because of its high solubility and excellent conductivity in alkyl carbonate solvents. Whereas, $LiPF_6$ is sensitive to trace amounts of moisture, resulting in by-products such as PF_5, POF_3, HF and LiF and $LiPF_6$ is of poor thermal stability. It starts to decompose at 40 ℃, and decomposes totally at 80 ℃[3,4]. Thus the side reactions of $LiPF_6$ make it difficult to meet the requirements of high energy density and long cycle life for hybrid electrical vehicle (HEV) application, especially in summer when the ambient temperature around lithium ion batteries for electrical vehicles will rise upto 70 ℃. Therefore, studies on new salts to replace $LiPF_6$ are attracting more and more attention now[5,6].

In 2006, Zhang[7] reported the chemical structure of LiODFB (molecular formula: $LiBC_2O_4F_2$ as shown in Fig.1) that possesses the combined advantages of LiBOB ($LiB(C_2O_4)_2$) and $LiBF_4$, and shows good electrochemical performances. He found that LiODFB could provide a high cycling efficiency for metallic lithium plating and stripping on the surface of Cu, and showed good passivation towards Al at high current rate. Recently, in high propylene carbonate (PC)-containing solutions, it is found that LiODFB used as electrolyte salt can provide stable SEI film and low cell impedance, which results in a dramatic improvement on both capacity retention and rate performance. Lithium ion batteries with LiODFB have excellent cycling performance even at 60 ℃[8,9]. Furthermore, it is found that the addition of small amount of LiODFB to the $LiPF_6$-based electrolyte can significantly improve both the capacity retention and the power retention of lithium ion batteries. But at the same time it will slightly increase the interfacial impedance of the cells[10]. So, thorough research on this salt needs to be done in order to get its widely commercial application.

LiODFB is attracted attention as soon as it was found because of its excellent electrochemical performances[11,12]. But at present research on it was just started, the electrochemical performances

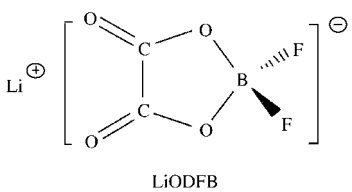

LiODFB

Fig.1 Molecular structure of LiODFB

of LiODFB in traditional solvents have not been reported. Therefore, LiODFB was dissolved in EC+DMC mixed solvents and was used as electrolyte. The performance behaviors of the Li/graphite (G) half cells and G/$LiCo_{1/3}Ni_{1/3}Mn_{1/3}O_2$ full cells using different two lithium salts were studied, and their interfacial characteristics were analyzed.

1 Experimental

1.1 Preparation of electrolyte

$LiPF_6$, LiODFB salts and EC, DMC solvents for application in batteries were purchased from Ferro Performance Materials Company, USA.

The solvents were purified further through RE-3000 rotary evaporator (made in Shanghai Yarong Company, China) and dried over 4A molecular sieves until the water content was lower than 2.0×10^{-5} (mass fraction), as determined by METTLER-TOLEDO DL32 Karl-Kisher titration (Mettler-Toledo Instruments Co. Ltd., Switz).

The base electrolytes used in this work, 1.0 mol·L^{-1} $LiPF_6$ in mass ratio of EC:DMC being 1:1 and 1.0 mol·L^{-1} LiODFB in mass ratio of EC:DMC being 1:1, were prepared in an Ar-filled glove box.

1.2 TG-DTA of the electrolyte salts

A SDTQ-600 simultaneous thermogravimetric analyzer (TA Instruments, USA) was used to analyze thermal stability and thermal behavior of LiODFB and $LiPF_6$ powders during heating. The samples LiODFB about 18.9960 mg and $LiPF_6$ about 24.1340 mg were heated from room temperature to 400 ℃ at a heating rate of 10 ℃·min^{-1} in nitrogen and argon mixture flow.

1.3 Constant current charge-discharge tests

The working electrode of half cells was composed of 94% (mass fraction) graphite and 6% poly(vinylidene difluoride) (PVDF) binder. The counter and reference electrodes of half cells were lithium foils. The separator was a Celgard 2400 microporous polylene membrane. The half cells were assembled using 2025 type coin cells and an appropriate amount of electrolyte in an Ar-filled glove box. The charge-discharge performances of Li/G half cells were evaluated at a constant current of 25 mA·g^{-1} (0.1*C*) with a voltage window 0–2.0 V(*vs* Li/Li^+) using a LAND CT2001A charge/discharge instrument (Wuhan Jinnuo Electronics Co. Ltd., China).

The positive electrode of full cells was composed of 84% (mass fraction) $LiCo_{1/3}Ni_{1/3}Mn_{1/3}O_2$, 8% carbon black and 8% PVDF binder. The negative electrode of full cells was composed of 94% (mass fraction) graphite (G) and 6% PVDF binder. The separator was a Celgard 2400 microporous polylene membrane. The full cells were assembled using 2025 type coin cells and an appropriate amount of electrolyte in an Ar-filled glove box. The initial charge-discharge capacity and cycling performance of G/$LiCo_{1/3}Ni_{1/3}Mn_{1/3}O_2$ cells were evaluated using a LAND CT2001A charge/discharge instrument. The charge cut-off and the discharge cut-off voltages were 4.2 and 2.5 V at a constant current of 0.1*C*, respectively. At the same case, the cells were cycled 100

times at high temperature (55 ℃) and were cycled 20 times at 0.5*C* and 1*C* rates at 25 ℃.

1.4 Electrochemical impedance tests

EIS was measured with 2025 type coin cells which were assembled according to the method in Section 2.3 in the PARSTAT 2273 electrochemical measurement system (Perkin Elmer Instrument, USA). The Li/G half cells using two kinds of different electrolytes were first discharged to 0.2 V with a constant current of 25 mA·g^{-1} (0.1*C*) before the electrochemical impedance of the cells was measured in the frequency range from 10 mHz to 100 kHz.

The G/$LiCo_{1/3}Ni_{1/3}Mn_{1/3}O_2$ full cells using two kinds of different electrolytes were first cycled between 3.0 and 4.0 V for two cycles with a constant current of 0.1*C*. Then the cells were constant-voltage-charged to 3.8 V before the electrochemical impedances were measured in the frequency range from 10 mHz to 100 kHz.

2 Results and discussion

2.1 Thermal stability analyses of $LiPF_6$ and LiODFB

The DTA-TG-DTG curves of $LiPF_6$ and LiODFB are given in Fig.2. In order to more directly analyze the thermogravimetry changes, the derivative thermogravimetry (DTG) curves of $LiPF_6$ and LiODFB are showed. The general information about their thermal behaviors, in terms of stability range, peak temperature and percentage mass loss, are presented in Table 1. As seen from Table 1, $LiPF_6$ show a two-step decomposition mode and LiODFB is three-step.

The first mass loss, which generally completes before 100 ℃ is related to the free acid removal. As seen in DTA-TG-DTG curves of Fig.2(A), the DTA profile of $LiPF_6$ salt shows that there is endothermic peak at about 76.85 ℃ between 43.19 and 82.75 ℃. Mass loss is about 4.25% at the stage which is the hydrogen fluoride removal. The thermal decomposition reaction is $LiPF_6 \cdot HF \rightarrow LiPF_6 + HF\uparrow$ [13]. Similarly, in DTA-TG-DTG curves of LiOD FB, there is less endothermic peak at about 68.54 ℃ in DTA curve of Fig.2(B) between 56.20 and 71.46 ℃. Mass loss is about 1.28% at the stage. Because the preparation techniques of LiODFB are not clear now, mass loss could be relate to the free acid in products. A low content of this acid in lithium salts is demanded for high-quality lithium-ion battery because the existence of free acid promotes severe corrosions of the current collectors, and leads to further deterioration of the battery performmance. The present work shows that the amount of the free acid in LiODFB salt is lower than that in $LiPF_6$.

Table 1 Decomposition temperature of TG-DTA

Salt	Stage	TG curve		Mass loss(%)	DTA curve
		T_i /℃	T_f /℃		T_p/℃
$LiPF_6$	I	43.19	82.75	4.25	76.85
	II	143.75	252.28	78.42	228.63
LiODFB	I	56.20	71.46	1.28	68.54
	II	219.33	295.47	41.93	276.29
	III	295.47	337.22	16.12	322.37

T_i, T_p, and T_f represent the initial decomposition temperature, the peak temperature of DTA, and the final decomposition temperature, respectively.

The main mass loss stage for the salt compounds is the decomposition of their base materials. From DTA curve of $LiPF_6$, it can be seen that there is obvious strong endothermic peak at about 228.63 ℃ in the temperature range of 143.75–252.28 ℃ and over. Mass loss is about 78.42% at the stage which is due to the completely decomposition reaction of $LiPF_6$: $LiPF_6 \rightarrow LiF + PF_5\uparrow$ [13]. Similarly, there is a big and acuate endothermic peak about 276.29 ℃ in DTA curve of LiODFB between 219.33 and 295.47 ℃. Mass loss is about 41.93% at the temperature range. Subsequently, there is less endothermic peak at about 322.37 ℃ in DTA curve of LiODFB between 295.47 and 337.22 ℃. Mass loss is about 16.12% in TG curve of LiODFB. These mass losses and endothermic peaks may be attribution to unique structure of LiODFB as shown in Fig.1. As indicated by its structure, LiODFB contains the same moieties as LiBOB and $LiBF_4$. The decomposition reaction of LiBOB at 302 ℃ is $2LiB(C_2O_4)_2 \rightarrow Li_2C_2O_4 + B_2O_3\uparrow + 3CO_2\uparrow + 3CO$[14]. The decomposition reaction of $LiBF_4$ at 162 ℃ is $LiBF_4 \rightarrow LiF + BF_3$[15]. Therefore the decomposition process of LiODFB may contain two decomposition reactions above.

From the above analysis, it can be seen that LiODFB has higher thermal stability and much less free acids and can not produce the poisonous PF_5 which high reacts with organic solvents in electrolyte. The released CO_2 may avoid thermal runway and possibly provides safety protection against abuse operations[7].

2.2 Elevated temperature cycling performances of G/$LiCo_{1/3}Ni_{1/3}Mn_{1/3}O_2$ cells

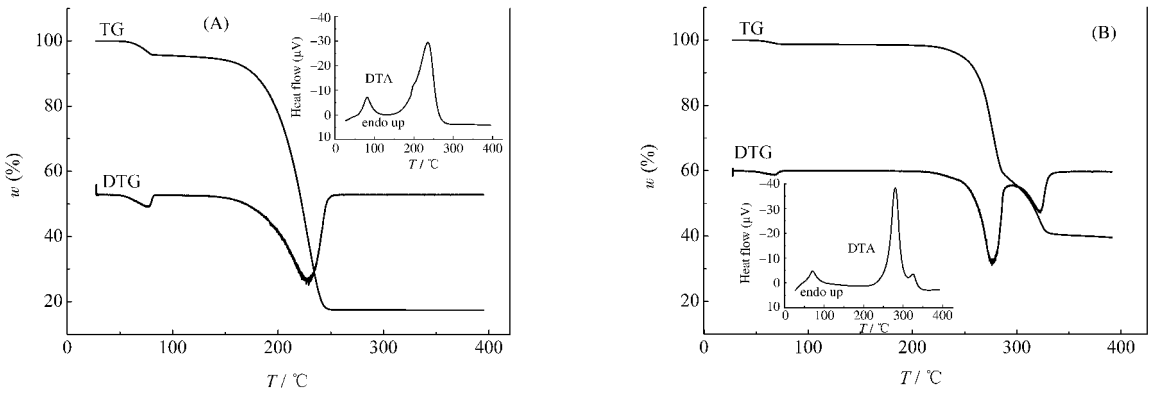

Fig.2 TG-DTA-DTG curves of $LiPF_6$ (A) and LiODFB (B)

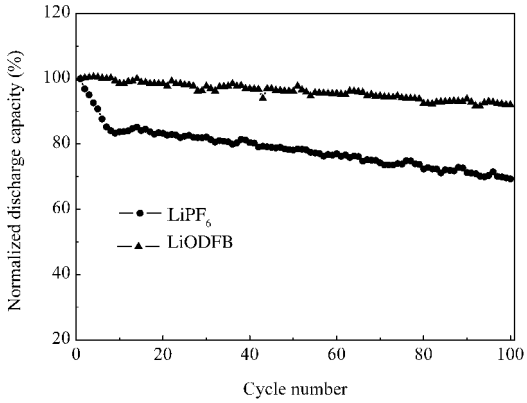

Fig.3 Capacity retention of G/$LiCo_{1/3}Ni_{1/3}Mn_{1/3}O_2$ full cells using different electrolytes at 0.1*C* rate and 55 ℃

Fig.3 shows the capacity retention of G/$LiCo_{1/3}Ni_{1/3}Mn_{1/3}O_2$ full cell at 55 ℃ with a constant current of 0.1*C*. It shows that LiODFB-based electrolyte has improved cycling performance. When the $LiPF_6$-based electrolyte is used, the cell′s capacity fades very fast. After 100 cycles, the loss of capacity is close to 31% at 55 ℃. When the LiODFB-based electrolyte is used, the cell′s capacity fades with only 8% after 100 cycles. The initial coulombic efficiency of the cell using the LiODFB-based electrolyte is higher than that of the cell using the $LiPF_6$-based electrolyte. It can be showed that the cells using the LiODFB-based electrolyte have not only excellent cycling performance but also higher initial coulombic efficiency. These are related to higher thermal stability of LiODFB salt. Then these advantages of LiODFB are analyzed from interfacial phenomenon with $LiPF_6$ counterpart.

2.3 Interface property of Li/G half cells

The SEI film layer plays the important role in protecting the graphite surfaces during subsequent cycling; the composition, morphology, and stability of the SEI film are known to critically affect the cycle- and storage-life of a lithium-ion cell[16,17]. Fig.4 shows the differential capacity profiles of Li/G half cells using different electrolytes. The cells were cycled at 25 ℃ with a constant current of 0.1*C*. Only the initial data showing the formation of SEI film are shown in Fig.4. Only one small peak about 0.65 V(*vs* Li/Li^+) is observed for the cell using $LiPF_6$-based electrolyte. This peak can also be observed for cells using LiODFB at a slightly higher potential. This peak is believed to be the result of the reduction of the alkyl carbonate solvents during passivation reaction on the graphite surfaces[18]. However, an extra strong peak is observed at about 1.5 V (*vs* Li/Li^+) for the cell using LiODFB. The peak is believed to be caused by the reduction and polymerization of $ODFB^-$. Liu *et al.*[10] thinks that the SEI film formed in the electrolyte without LiODFB has more inorganic components (such as Li_2CO_3 and LiF) that are less sensitive to the temperature, while the SEI film formed with the electrolyte with LiODFB has more organic components that are more sensitive to temperature and has lower impedance at elevated temperature. This is beneficial to both remaining higher cycling capacity retention and less initial capacity loss of the cells at high temperature (Fig.3).

Graphite negative interfacial impedance is the main contributor to full cell impedance[1]. In order to further confirm electrolyte salt effect on interface impedance of surface graphic negative, AC impedances of Li/G half cells using different electrolytes are studied and shown in Fig.5. In all case, the EIS shows either one semicircle or two partially overlapped semicircles, followed by a straight sloping line at the low frequency end. The high frequency semicircle of EIS is resistance of the SEI film on the surface of graphite. The medium frequency semicircle is the charge-transfer resistance. The following straight sloping line at low frequency end is mainly related to diffusion process of lithium ions on the electrode-electrolyte interface. In the potential regions where no electrode reactions take place, the resistance which corresponds to the medium frequency semicircle is so high that its related semicircle disappears, and in this case, the EIS shows only one semicircle followed by a straight sloping line. SEI film can be studied by different semicircles, as shown by Nyquist profiles of EIS in Fig.5. The data show that the cells using $LiPF_6$ have a lower interfacial impedance, about 12 Ω at 0.2 V. The cells using LiODFB-based electrolyte have a slightly higher impedance, about 17 Ω at 0.2 V, because alkyl carbonate electrolytes form a preliminary SEI film on the graphic surface in the 0.6–0.7 V range before graphic lithiation at 0.2 V[19]. But LiODFB at 1.5 V

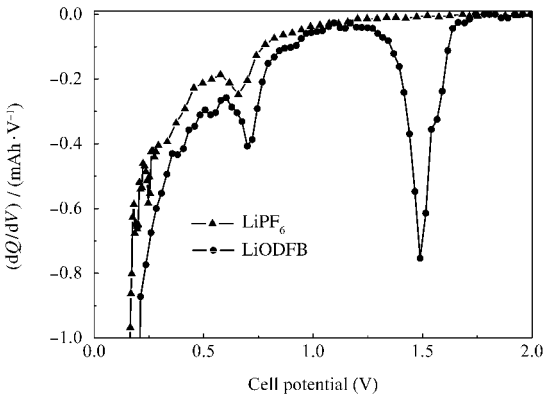

Fig.4 First charge differential capacity profiles of Li/G half cells with different electrolytes

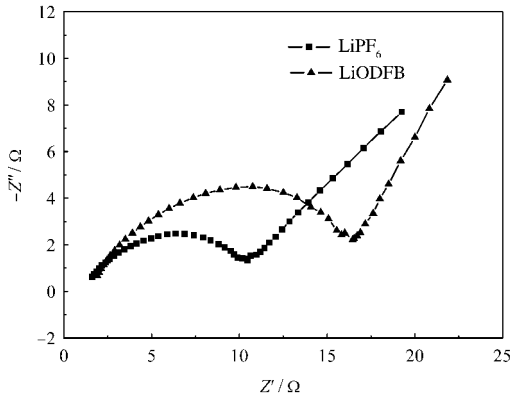

Fig.5 Nyquist profiles of AC impedance of Li/G half cells with different electrolytes

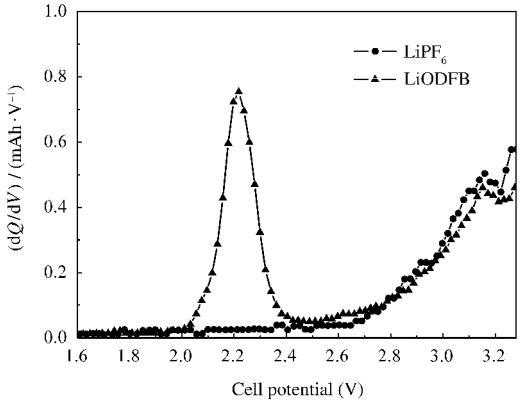

Fig.6 First charge differential capacity profiles of G/$LiCo_{1/3}Ni_{1/3}Mn_{1/3}O_2$ full cells with different electrolytes

causes the reduction and polymerization and participates in the SEI film formation that lead to improve thickening of film and increase impedance of film[20], which is disadvantageous to improve power capability of the cells.

2.4 Interface property of G/$LiCo_{1/3}Ni_{1/3}Mn_{1/3}O_2$ full cells

The differential capacity profiles of G/$LiCo_{1/3}Ni_{1/3}Mn_{1/3}O_2$ full cells using different electrolytes are shown in Fig.6. The cells were charged at 25 ℃ with a constant current of 0.1*C*, and only the initial data below 3 V during the first charge are shown in Fig.6 to demonstrate the impact of LiODFB on the SEI film formaton. A small peak is observed at about 3.0 V for each electrolyte profile and the peak position is almost the same. This peak can be further related to the peak at 0.65 V in half cells (Fig.4). The peak with large intensity is observed at about 2.2 V for the cell containing LiODFB, but not for the cell containing $LiPF_6$. LiODFB dose not participate in the electrochemical reaction on the positive electode through the electrochemical reaction[10]. Hence, it can be concluded that the peak at 2.2 V is believed to result from the SEI film layer formed by the LiODFB, and the peak is also related to the extra peak at 1.5 V in half cell containing LiODFB. This shows that LiODFB forms a protective film on the negative electrode during the initial charge-discharge process from being attacked by other cell components.

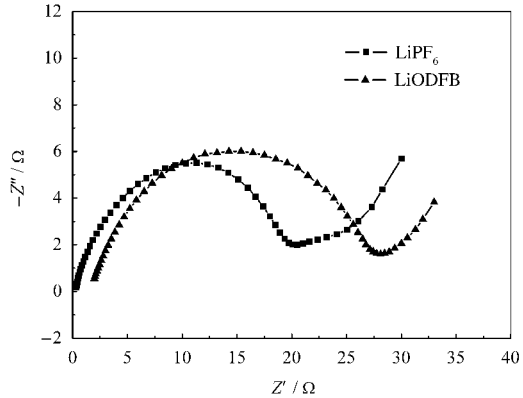

Fig.7 Nyquist profiles of AC impedance of G/$LiCo_{1/3}Ni_{1/3}Mn_{1/3}O_2$ full cells with different electrolytes

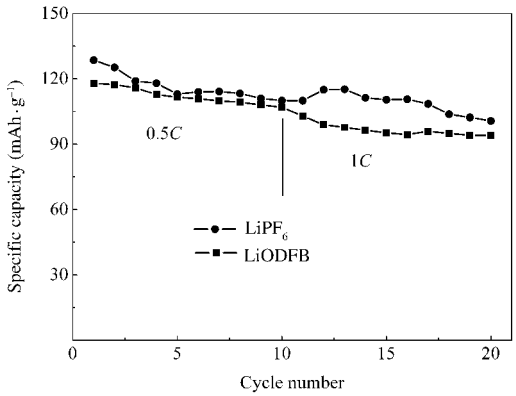

Fig.8 Cycling performances of G/$LiCo_{1/3}Ni_{1/3}Mn_{1/3}O_2$ full cells using different electrolytes at different discharge rates and 25 ℃

Nyquist profiles of AC impedance of G/$LiCo_{1/3}Ni_{1/3}Mn_{1/3}O_2$ f ull cells with different electrolytes are shown in Fig.7. The full cell using LiODFB-based electrolyte has an impedance of about 27 Ω, which is 17% slightly higher than that of the full cell using $LiPF_6$-based electrolyte (about 23 Ω), as shown in Fig. 7. Therefore, this suggests that the power capability of the G/$LiCo_{1/3}Ni_{1/3}Mn_{1/3}O_2$ full cells could be slightly reduced by completely replacing $LiPF_6$ with LiODFB.

2.5 Rate performances of G/$LiCo_{1/3}Ni_{1/3}Mn_{1/3}O_2$ full cells

In order to further confirm rate performance, Fig.8 shows the electrochemical performances of the G/$LiCo_{1/3}Ni_{1/3}Mn_{1/3}O_2$ full cells using the two different electrolytes at 0.5*C* and 1*C* discharge rates. At 0.5*C* and 1*C* discharge rates, the rate capability of the cell with the LiODFB-based electrolyte is almost the same as that of the cell with the $LiPF_6$-based electrolyte, and the gap between the two cells was tiny. The initial discharge capacity of the cell using the $LiPF_6$-based electrolyte is higher, about 128.6 $mAh \cdot g^{-1}$. After 20 cycles, the discharge capacity is still 100.7 $mAh \cdot g^{-1}$, the capacity retention is 78.3%. While about 117.6 $mAh \cdot g^{-1}$ of the initial discharge capacity of the cell using the LiODFB-based electrolyte decreases to 94.1 $mAh \cdot g^{-1}$ after 20 cycles, the capacity retention is 80.0%. The capability fade of the latter is even slower than that of the former. It is very clear that the cells using LiODFB provides a slightly higher impedance of SEI film that leads to a slightly lower rate capacity, and a protective film on surface of anode that leads to better coulombic efficiency and cycling capacity retention. In summary, the cells using the LiODFB-based electrolyte can provide better comprehensive performances.

3 Conclusions

(1) LiODFB has higher thermal stability and much less free acid content, and released CO_2 possibly provides good safety of cells.

(2) The cells using LiODFB-based electrolyte have lower capacity fade than the cells using $LiPF_6$-based electrolyte after 100 cycles at 55 ℃, and higher initial capacity retention at the elevated temperature.

(3) At 0.5*C* and 1*C* discharge rates, the rate capability of the cells with the LiODFB-based electrolyte is almost the same as that of the cells with the $LiPF_6$-based electrolyte after 20 cycles, and the gap between the two cells is tiny.

(4) Interface properties of the cells show that LiODFB is reduced and forms a thickening and protective SEI film on the negative electrode. Although this can increase the impedance of SEI film, the cells still can provide a preferable rate performance. More work is needed to carry out in the lithium battery of commercialization in the future.

References

1 Abraham, D. P.; Furczon, M. M.; Kang, S. H.; Dees, D. W.; Jansen, A. N. *J. Power Sources*, **2008, 180**(1): 612

2 Li, F. Q.; Lai, Y. Q.; Zhang, Z. A.; Gao, H. Q.; Yang, J. *Acta Phys.-Chim. Sin*., **2008, 24**(7): 1302 [李凡群, 赖延清, 张治安, 高宏权, 杨 娟. 物理化学学报, **2008, 24**(7): 1302]

3 Amine, K.; Liu, J.; Kang, S.; Belharouak, I.; Hyung, Y.; Vissers, D.; Henriksen, G. *J. Power Sources*, **2004, 129**(1): 14

4 Andersson, A. M.; Edström, K. *J. Electrochem. Soc*., **2001, 148** (10): A1100

5 Sasaki, Y.; Handa, M.; Sekiya, S.; Kurashima, K.; Usami, K. *J. Power Sources*, **2001, 97/98**: 561

6 Yu, B. T.; Qiu, W. H.; Li, F. S.; Xu, G. X. *Electrochemical and Solid-State Letters*, **2006, 9**(1): A1

7 Zhang, S. S. *Electrochem. Commun*., **2006, 8**(9): 1423

8 Aravindan, V.; Vickraman, P.; Krishnaraj, K. *Polymer International*, **2008, 57**(7): 932

9 Aravindan, V.; Vickraman, P. *Solid State Sciences*, **2007, 9**(11): 1069

10 Liu, J.; Chen, Z. H.; Busking, S.; Amine, K. *Electrochem. Commun*., **2007, 9**(3): 475

11 Kang, S. H.; Abraham, D. P.; Xiao, A.; Lucht, B. L. *J. Power Sources*, **2008, 175**(1): 526

12 Zhang, S. S. *J. Power Sources*, **2007, 163**(2): 713

13 Smagin, A. A.; Matyukha, V. A.; Korobtsev, V. P. *J. Power Sources*, **1997, 68**(2): 326

14 Xu, K.; Zhang, S. S.; Jow, T. R.; Xu, W.; Angell, C. A. *Electrochemical and Solid-State Letters*, **2002, 5**(1): A26

15 Lu, Z. R.; Yang, L.; Guo, Y. J. *J. Power Sources*, **2006, 156**(2): 555

16 Zheng, T.; Gozdz, A. S.; Amatucci, G. G. *J. Electrochem. Soc*., **1999, 146**(11): 4014

17 Herstedt, M.; Abraham, D. P.; Kerr, J. B.; Edström, K. *Electrochim. Acta*, **2004, 49**(28): 5097

18 Chen, Z. H.; Lu, W. Q.; Liu, J.; Amine, K. *Electrochim. Acta*, **2006, 51**(16): 3322

19 Zheng, H. H. Electrolyte of lithium ion battery. Beijing: Chemical Industry Press, 2007: 80 [郑洪河. 锂离子电池电解质. 北京: 化学工业出版社, 2007: 80]

20 Zhang, S. S.; Xu, K.; Jow, T. R. *Electrochim. Acta*, **2006, 51**(8/9): 1636